Letter

Hydrodynamic instabilities in driven chiral suspensions

Seema Chahal [*] and Brato Chakrabarti [†]
International Centre for Theoretical Sciences, Tata Institute of Fundamental Research, Bengaluru 560089, India

(Received 29 August 2025; accepted 5 February 2026; published 26 February 2026)

Active Stokesian suspensions are conventionally understood to generate dipolar stresses that destabilize aligned states in the bulk and drive systemwide spatiotemporally chaotic flows. Here, we report dynamics in suspensions of torque-driven spinning chiral particles that exhibit a distinct and previously unrecognized route to collective dynamics. Using a mean-field kinetic theory, stability analysis, and nonlinear simulations, we demonstrate how flows driven by torque monopoles and self-propulsion resulting from microscopic chirality drive chaotic flows in three dimensions. Unlike the well-known alignment instability of dipolar active matter, the present dynamics is intrinsically tied to self-propulsion and relies on the emergent coupling between nematic and polar order. Our results establish a novel route to pattern formation, suggest strategies for designing torque-driven active suspensions, and provide a mechanistic framework to probe the rheology of chiral fluids.

DOI: 10.1103/9kfb-c51g

Microorganisms, active cytoskeletal structures, and their synthetic analogs perform mechanical work on their surroundings by consuming chemical energy. This activity typically results in dipolar stresses, a hallmark of force-free active particles. It is well known that a bulk, momentum-conserving suspension of such dipolar active particles are susceptible to the "generic" alignment instability which renders a Stokesian flock unstable beyond a critical activity, leading to states of spontaneous flow and chaotic dynamics [1–6]. This instability has become the hallmark and defining route to collective dynamics in active Stokesian fluids [7–9]. In this letter, we focus on a distinct class of active, or rather driven, suspensions comprising particles that do not produce dipolar stresses. Instead, each particle spins around its body axis under the action of external torque and thus acts as a torque monopole in the bulk fluid [10]. For such systems, the generic route to pattern formation is absent. However, we uncover a new pathway to collective dynamics that arises when the particles are chiral. The microscopic screwlike chirality results in self-propulsion along the spinning axis, which in turn triggers an instability unique to self-propelled particles, leading to emergent systemwide flows in three-dimensional suspensions. Our results reveal a previously unrecognized mode of self-organized flows, with potential implications for engineered driven suspensions [11,12] and rheology of chiral fluids [13].

Chirality is a pervasive feature of biological and synthetic active systems [14]. Examples range from the clockwise swimming of surface-bound *E. coli* [15], to rotating cilia [16], and chiral actomyosin flows [17,18] at the cell cortex, each illustrating how molecular chirality shapes emergent large-scale dynamics. Another prominent manifestation of chirality is the coupling between translation and rotation, seen in the spinning propulsion of cytoskeletal filaments in gliding assays [19], the swimming of *E. coli* driven by their helical flagella [20], and the engineered motion of driven helical micromotors [12]. Most prior theoretical and experimental work on collective manifestation of chirality have focused on quasi-two-dimensional settings [21], including layered [22,23] and nematic materials [24], or spinning collectives confined to a plane [25,26]; only recently has the role of chirality been probed in three-dimensional dry active matter [27]. While a recent hydrodynamic framework addressed the surface motility of the rod-shaped bacterium *Myxococcus xanthus*, which spins its body to glide on substrates [28], the dynamics of momentum-conserving bulk suspensions of torqued chiral particles, where rotation and translation are aligned, remain unknown.

Here, we combine theory and simulations to unravel a range of new hydrodynamic instabilities for spinning, chiral elongated particles that exert a torque monopole along their long axis [Fig. 1(a)]. Such a hydrodynamic signature is in contrast with truly active particles (for example, a bacterium) with an internal source of energy that are torque free and hence exert a torque dipole in the bulk [20]. Thus, the particles under consideration in this letter are driven or actuated by external means [12]. One approach to experimentally realizing a torque-driven suspension is to harness electrohydrodynamic instabilities such as Quincke rotations of dielectric particles in a bulk fluid [29]. Such dynamics have been reported experimentally [30,31] for isolated spheroids and theoretically for chiral particles such as helices that propel along their spinning axis [32]. Here, we demonstrate how such microscopic chirality and fluid-mediated long-range interactions resulting from torque monopoles conspire to drive instabilities in dilute suspensions of these chiral particles.

Modeling. We start by laying out our model, which builds on a mean-field kinetic theory for spheroidal particles suspended in a Stokesian fluid [2]. Here, we consider an idealized setup in which each particle is actuated individually by externally applied local torques along its long axis; the actuation

[*]Contact author: seema.s@icts.res.in
[†]Contact author: brato.chakrabarti@icts.res.in

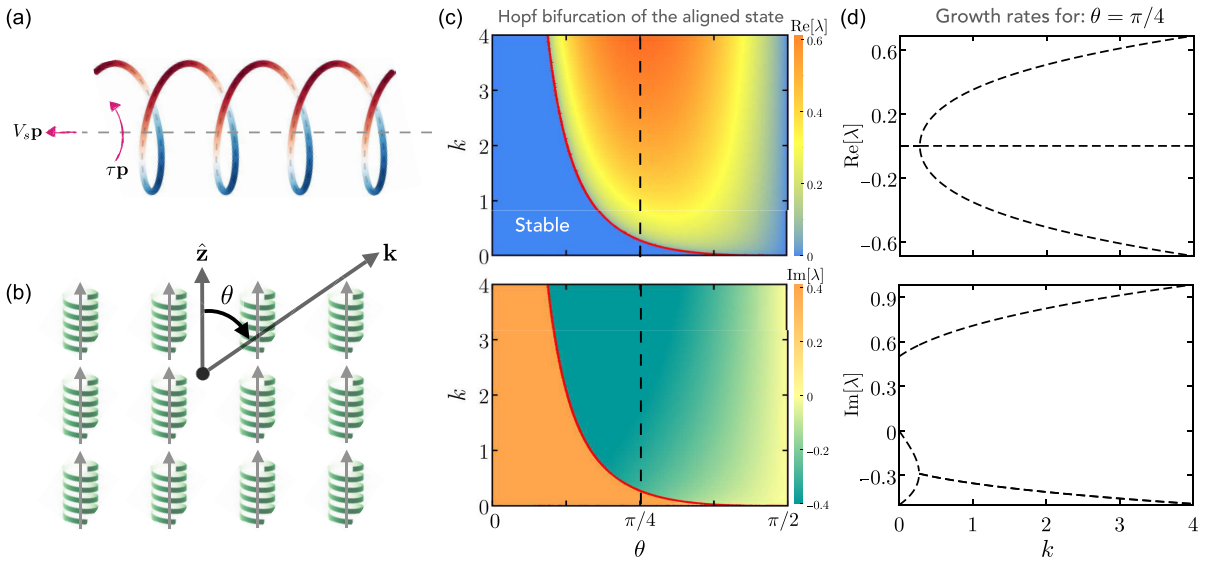

FIG. 1. (a) Screwlike chiral particles are actuated along their long axis by external torque $\tau\mathbf{p}$. Translation-rotation coupling causes each particle to both spin and self-propel along $\mathbf{p}$. (b) Illustration of the uniaxial (polar) phase of the suspension and the perturbation wave vector $\mathbf{k}$. Because the particle stress is polar, the stability of apolar-nematic states differs from that of the polar states analyzed here [39]. (c) Dispersion relation of the most unstable eigenvalue in the k-θ space. The real part of the growth rate (top panel) shows a finite k instability beyond the red stability boundary. Imaginary parts (bottom panel) illustrate that the instability carries the signature of a Hopf bifurcation. (d) Dispersion relation as a function of wave number k for a given $\theta = \pi/4$ [dashed line in (c)]. The three branches correspond to the numerically obtained eigenvalues of the linearized problem. For all the analyses shown here we chose $d_T = d_r = 0$ and $\chi = 1$.

does not arise from a global external field and therefore does not introduce an explicit symmetry breaking on the unit sphere. The suspension is described by a probability density function $\Psi(\mathbf{x}, \mathbf{p}, t)$ that encodes the probability of finding a particle at position $\mathbf{x}$ with director $\mathbf{p} \in \mathbb{S}^2$ (the unit sphere) characterizing the orientation of the long axis of the particle at time t. The distribution function obeys a conservation equation

$$\frac{\partial \Psi}{\partial t} + \nabla_{\mathbf{x}} \cdot (\dot{\mathbf{x}}\Psi) + \nabla_{\mathbf{p}} \cdot (\dot{\mathbf{p}}\Psi) = 0, \tag{1}$$

where $\Psi(\mathbf{x}, \mathbf{p}, t)$ is normalized as

$$\frac{1}{V}\int_V d\mathbf{x} \int_{\mathbb{S}^2} d\mathbf{p}\, \Psi(\mathbf{x}, \mathbf{p}, t) = \bar{n}, \tag{2}$$

with $\bar{n}$ being the mean number density of the particles. In Eq. (1), $\nabla_{\mathbf{p}} = (\mathbf{I} - \mathbf{pp}) \cdot \partial_{\mathbf{p}}$ is the gradient operator on the unit sphere, and $\dot{\mathbf{x}}$ and $\dot{\mathbf{p}}$ are respectively the translational and rotational flux velocities given by

$$\dot{\mathbf{x}} = V_s\mathbf{p} + \mathbf{u}(\mathbf{x}) - D_T \nabla_{\mathbf{x}} \ln \Psi, \tag{3}$$

$$\dot{\mathbf{p}} = (\mathbf{I} - \mathbf{pp}) \cdot (\gamma\mathbf{E} + \mathbf{W}) \cdot \mathbf{p} - D_r \nabla_{\mathbf{p}} \ln \Psi. \tag{4}$$

In Eq. (3) V_s is the self-propulsion speed of the particles, $\mathbf{u}(\mathbf{x})$ is the self-generated mean-field velocity arising due to the particle stress in the suspension, and D_T is the translational diffusion coefficient. Note that $V_s \neq 0$ only for chiral particles: due to microscopic chirality, the self-propulsion speed is intrinsically linked and proportional to the actuating torque on the particle. Such a propulsion mechanism differs from the well-studied dipolar active particle, such as a microswimmer, where the swimming speed can be independent of its far-field signature of dipolar flows. To model the orientational dynamics of the particles in Eq. (4) we used Jeffery's equation [33], where γ is a geometric parameter characterizing the shape anisotropy and D_r is the rotational diffusion coefficient; $\{\mathbf{E}, \mathbf{W}\}$ are the symmetric and antisymmetric parts of the mean-field velocity gradient tensor. While Jeffery's equation is appropriate for homochiral particles, recent work has identified higher-order corrections for other chiral shapes [34,35]; chirality may also induce a weak drift of the particle's center of mass [36]. We ignore such effects for simplicity. Here, we restrict ourselves to a dilute suspension with $\bar{n}\ell_p^3 \ll 1$, where ℓ_p is the characteristic length of our active particles; in this dilute limit, the mean-field flow $\mathbf{u}(\mathbf{x})$ is self-consistently computed from a forced incompressible Stokes equation as

$$-\nabla q + \mu\Delta\mathbf{u} + \nabla \cdot \boldsymbol{\Sigma}^{\mathrm{a}} = \mathbf{0}, \quad \nabla \cdot \mathbf{u} = 0, \tag{5}$$

where q is the pressure and $\boldsymbol{\Sigma}^{\mathrm{a}}$ is a particle stress on the fluid due to the presence of torque monopoles along the axis of our particles. Following Refs. [37,38], the volume-averaged particle stress at $\mathbf{x}$ is given as [39]

$$\Sigma^{\mathrm{a}}_{ij}(\mathbf{x}, t) = \frac{\tau}{2}\int_{\mathbb{S}^2} \epsilon_{ijk} p_k \Psi(\mathbf{x}, \mathbf{p}, t)\, d\mathbf{p} = \frac{\tau}{2}\epsilon_{ijk} c n_k. \tag{6}$$

Here, τ is the magnitude of the external actuating torque acting along the long axis and ϵ is the Levi-Civita tensor. In Eq. (6), we have also defined the mean-field density and polarity field as $c = \int_{\mathbb{S}^2} \Psi(\mathbf{x}, \mathbf{p}, t) d\mathbf{p}$ and $\mathbf{n} = 1/c \int_{\mathbb{S}^2} \mathbf{p}\Psi(\mathbf{x}, \mathbf{p}, t) d\mathbf{p}$. We highlight that each spinning particle in our problem acts as a rotlet and the resulting particle stress $\boldsymbol{\Sigma}^{\mathrm{a}}$ is antisymmetric as required from the conservation of angular momentum. Importantly, the particle stress

is also polar in contrast to the familiar symmetric nematic active stresses that depend on the nematic order. The above equations can be made dimensionless using the following velocity, length, and timescales: $u_c \sim \tau/2\mu\ell_p^2$, $l_c \sim (\bar{n}\ell_p^2)^{-1}$, and $t_c \sim l_c/u_c$. After the above scaling, we are left with dimensionless diffusivities $d_T = D_T/(l_c u_c)$ and $d_r = D_r l_c/u_c$, and a geometric factor $\chi = V_s/u_c \sim \mathcal{O}(1)$ that depends on the microscopic chirality and associated mobility of individual particles, capturing the intrinsic coupling between self-propulsion and the torque monopole [39]. The number density $\bar{n}$ only appears in our problem through the system size scaled by the $(\bar{n}\ell_p^2)^{-1}$. Equations (1)–(6) thus provide us with a self-consistent evolution problem for $\Psi(\mathbf{x}, \mathbf{p}, t)$; in this micro-macro framework, the actuation of the particles by external torque forces the Stokesian fluid, which in turn affects their collective distribution. We now examine how these hydrodynamic interactions, combined with microscopic chirality, can drive instabilities and pattern formation in such suspensions.

Linear stability analysis. To highlight the possible emergent dynamics, we first study the dynamics of a uniaxial, aligned state of spinning particles. In particular, we consider a nematic and polar state of the suspension described by $\Psi(\mathbf{x}, \mathbf{p}, t) = c(\mathbf{x}, t)\delta[\mathbf{p} - \mathbf{n}(\mathbf{x}, t)]$ around which the evolution of c and $\mathbf{n}$ follows,

$$\frac{\mathrm{D}c}{\mathrm{D}t} + \chi\nabla\cdot(\mathbf{n}c) - d_T\Delta c = 0, \tag{7}$$

$$\frac{\mathrm{D}\mathbf{n}}{\mathrm{D}t} + \chi\mathbf{n}\cdot\nabla\mathbf{n} - d_T\Delta\mathbf{n} = \mathcal{P}_\mathbf{n}\cdot(\gamma\mathbf{E} + \mathbf{W})\cdot\mathbf{n}. \tag{8}$$

Here, $\mathrm{D}/\mathrm{D}t = \partial_t + \mathbf{u}\cdot\nabla$ is the material derivative, $\mathcal{P}_\mathbf{n} = (\mathbf{I} - \mathbf{nn})$ is a projection operator, and we have ignored rotational diffusion. The homogeneous, aligned state with $c_0 = 1$ and $\mathbf{n} = \mathbf{n}_0$ is a fixed point of the problem with the mean-field velocity $\mathbf{u}(\mathbf{x}) = \mathbf{0}$. To probe the stability of this fixed point we use plane-wave perturbations of the following form, $c = 1 + \varepsilon\tilde{c}_k e^{\mathrm{i}\mathbf{k}\cdot\mathbf{x}+\sigma t}$ and $\mathbf{n} = \hat{\mathbf{z}} + \varepsilon\tilde{\mathbf{n}}_k e^{\mathrm{i}\mathbf{k}\cdot\mathbf{x}+\sigma t}$ with $|\varepsilon| \ll 1$. Here, $\mathbf{k}$ is the wave vector and σ is the growth rate of the perturbation; furthermore, we have assumed $\mathbf{n}_0 = \hat{\mathbf{z}}$ without any loss of generality with $\tilde{\mathbf{n}} = \{\tilde{n}_1, \tilde{n}_2, 0\}$. Retaining terms up to $\mathcal{O}(\varepsilon)$, we linearize Eqs. (7) and (8) and solve for the perturbed mean-field velocity from Eq. (5) in Fourier space to obtain an eigenvalue problem for the growth rate σ as

$$\begin{aligned}
\lambda\tilde{c} &= -\mathrm{i}\chi k\cos\phi\sin\theta\tilde{n}_1 - \mathrm{i}\chi k\sin\phi\sin\theta\tilde{n}_2,\\
\lambda\tilde{n}_1 &= -\sin\phi\cos\theta\sin\theta\tilde{c} + \cos^2\theta\tilde{n}_2,\\
\lambda\tilde{n}_2 &= \cos\phi\cos\theta\sin\theta\tilde{c} - \cos^2\theta\tilde{n}_1.
\end{aligned} \tag{9}$$

Here, $\{\theta, \phi\}$ are respectively spherical polar and azimuthal angles with $\theta = \cos^{-1}(\mathbf{k}\cdot\hat{\mathbf{z}}/k)$ where $k = |\mathbf{k}|$ (Fig. 1); a modified eigenvalue is defined as $\lambda = (\sigma + \mathrm{i}k\cos\theta + d_T k^2)$. Hereafter, we have assumed $\gamma = 1$ corresponding to elongated rodlike particles [39]. The solution to this eigenvalue problem reveals a Hopf bifurcation of the aligned state with a nontrivial dependence on the wave number k and the direction of perturbation characterized by the polar angle θ [Fig. 1(c)]. In particular, the long-wavelength modes with $k = 0$ are stable (or marginal in the absence of translational diffusion) with the instability emerging at finite k. This wave-number selection is in contrast with the generic alignment instability [7] that

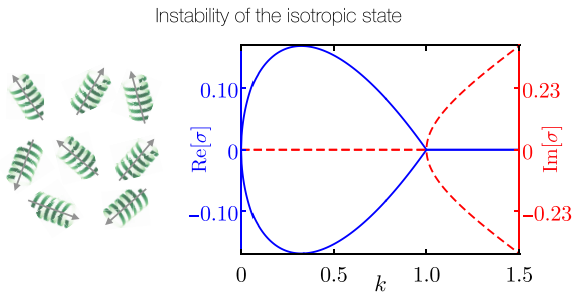

FIG. 2. Dispersion relation for the isotropic state depicted pictorially on the left. Here, we have chosen $d_T = d_r = 0$ and $\chi = 1$.

predicts a scale-free, long-wavelength pitchfork bifurcation of the bulk uniaxial phase [40,41]. Furthermore, we find that perturbations that are exactly aligned with the flock ($\theta = 0$) or transverse to the flock ($\theta = \pi/2$) are stable. While the linear theory predicts that for unstable modes, the growth rate increases with k [Fig. 1(d)], in practice, such high wave numbers are cut off due to translational diffusion (or nematic elasticity). Finally, and perhaps most importantly, the predicted instability is absent if $V_s \sim \chi = 0$. Thus, for achiral, spinning particles that do not self-propel, the aligned state is always stable. We now probe the stability of another fixed point of our system: the homogeneous, isotropic state of the suspension with $\Psi_0 = 1/4\pi$ and $\mathbf{u}(\mathbf{x}) = \mathbf{0}$. In this isotropic state, we still assume that individual particles spin along their long axis due to external actuations and propel along their backbone $\mathbf{p}$ as a result of the microscopic chirality. To analyze the stability, we perturb the distribution

$$\Psi(\mathbf{x}, \mathbf{p}, t) = \frac{1}{4\pi}[1 + \varepsilon\Psi'(\mathbf{x}, \mathbf{p}, t)], \quad |\varepsilon| \ll 1. \tag{10}$$

Substituting the above expression in Eq. (1) and retaining terms up to $\mathcal{O}(\varepsilon)$ we arrive at the following evolution equation for the perturbation,

$$\frac{\partial\Psi'}{\partial t} = -\chi\mathbf{p}\cdot\nabla_\mathbf{x}\Psi' + d_T\Delta\Psi' + 3\mathbf{pp} : \mathbf{E}', \tag{11}$$

where $\mathbf{E}'$ is the perturbed rate-of-strain tensor and we have set $d_r = 0$ for simplicity. As above, we consider a plane-wave ansatz as $\Psi'(\mathbf{x}, \mathbf{p}, t) = \tilde{\Psi}(\mathbf{p}, \mathbf{k})e^{\mathrm{i}\mathbf{k}\cdot\mathbf{x}+\sigma t}$ and obtain a nonlinear dispersion relation [39] for unknown growth rate σ as

$$\left[2a^2 - \frac{4}{3} + (a^3 - a)\log\left(\frac{a-1}{a+1}\right)\right] = \pm\frac{4}{3}\chi k, \tag{12}$$

where $a = -\mathrm{i}(\sigma + d_T k^2)/\chi k$. Figure 2 shows the real and imaginary parts of the numerically obtained growth rate $\sigma(k)$, which, owing to the isotropy of the base state, is independent of wave-vector direction. The data reveal a clear wave-number selection, with the long-wavelength limit ($k = 0$) remaining stable. In line with our earlier analysis of the aligned state, the instability emerges only when the particles are self-propelled ($\chi \neq 0$).

Features of the instability. Our linear analysis uncovers an alignment instability in both the ordered and isotropic states of the suspension. Two key features distinguish this instability from that in conventional active suspensions: (i) long-wavelength modes are suppressed in the bulk, and (ii) the

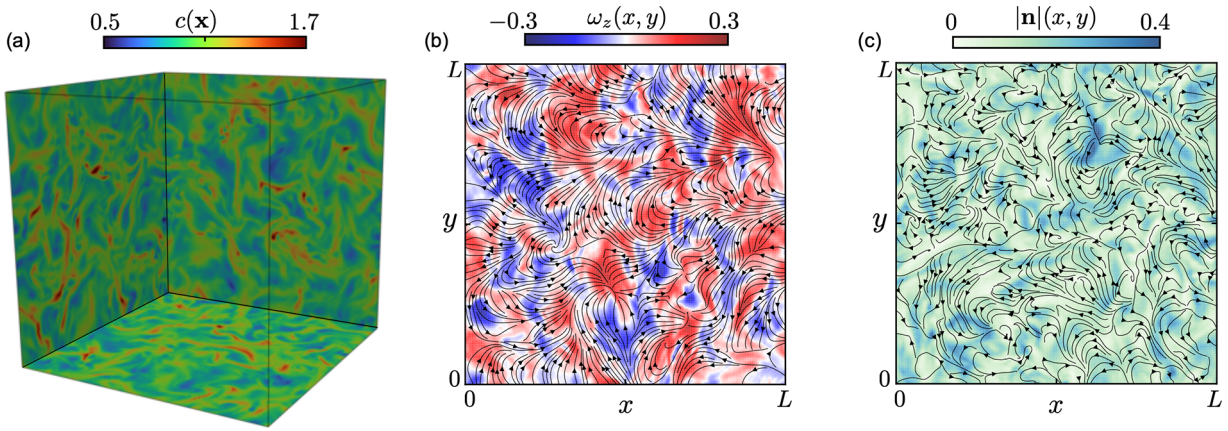

FIG. 3. Snapshots from a statistically steady state of a 3D direct numerical simulation of the moment equations in a triply periodic square box of size L. (a) Concentration field on three faces of the periodic box, revealing fluctuations and formation of bands. (b) Highlights the mean-field velocity streamlines in a 2D slice (x-y plane) from the 3D simulation. The background is color coded by the out-of-plane vorticity field ω_z. The patches in the vorticity field evolve continuously and exhibit spatiotemporally chaotic patterned states reminiscent of low Reynolds number active turbulence [47]. (c) The polarity field and its magnitude on the same 2D slice as in (b). Starting from an initially isotropic state, the system develops regions of high polarity. Parameters: $L = 50\pi$, $\chi = 0.5$, $d_T = 0.01$, $d_r = 0.01$; each spatial direction was discretized using $N = 128$ points.

suspension remains stable in the absence of self-propulsion. The latter feature renders the instability unique to chiral screws, which self-propel as they spin.

To understand the origin of these defining features, we examine the instability of the isotropic state in detail. Velocity fluctuations about this state induce nematic ordering of the particles along the extensional axis of the flow perturbations. The ordering is nematic because Jeffery's equation, which governs their orientational dynamics, is invariant under the transformation $\mathbf{p} \to -\mathbf{p}$ [3]. In extensile bacterial suspensions, such nematic ordering amplifies velocity fluctuations via dipolar stresses, eventually resulting in an instability. By contrast, in the present system, the particle stress is polar, and velocity fluctuations can only grow if nematic order generates local polar order. Crucially, this nematopolar coupling arises only for self-propelled particles as previously recognized in Ref. [42]. To illustrate this explicitly, we consider the evolution equations for the concentration c, polarity $\mathbf{n}$, and the nematic order field $\mathbf{Q}$ given as

$$\partial_t c + \boldsymbol{\nabla} \cdot [(\mathbf{u} + \chi \mathbf{n})c] - d_T \Delta c = 0, \tag{13}$$

$$(c\mathbf{n})^{\nabla} + \chi \boldsymbol{\nabla} \cdot (c\mathbf{Q}) - d_T \Delta(\mathbf{n}c) = -c\mathbf{R} : \mathbf{E}, \tag{14}$$

$$(c\mathbf{Q})^{\nabla} + \chi \boldsymbol{\nabla} \cdot (c\mathbf{R}) - d_T \Delta(\mathbf{Q}c) = -2c\mathbf{S} : \mathbf{E}, \tag{15}$$

where $\mathbf{Q} = \langle \mathbf{pp}\Psi \rangle / c$; $\mathbf{R} = \langle \mathbf{ppp}\Psi \rangle / c$ and $\mathbf{S} = \langle \mathbf{pppp}\Psi \rangle / c$ are higher-order moments of the particle distribution and $\langle (\cdot) \rangle = \int_{\mathbb{S}^2} (\cdot) \mathrm{d}\mathbf{p}$ denotes orientational averages. We have also defined the upper convected derivative of a vector as $\mathbf{a}^{\nabla} = \mathrm{D}_t \mathbf{a} - \boldsymbol{\nabla}\mathbf{u} \cdot \mathbf{a}$ and a tensor as $\mathbf{A}^{\nabla} = \mathrm{D}_t \mathbf{A} - (\boldsymbol{\nabla}\mathbf{u} \cdot \mathbf{A} + \mathbf{A} \cdot \boldsymbol{\nabla}\mathbf{u}^T)$. It follows from Eq. (14) that when $V_s \sim \chi = 0$, the polar order remains decoupled from nematic ordering potentially induced by velocity fluctuations. As a result, the isotropic state with $\mathbf{n}_0 = \mathbf{R}_0 = \mathbf{0}$ remains a stable fixed point of the problem; thus, suspensions of achiral, spinning particles are stable [43]. Furthermore, at linear order, the growth of polar order is related to fluctuations in $\mathbf{Q}$ as $\partial_t n_\alpha \sim \chi \nabla_\beta Q_{\alpha\beta} \equiv \mathrm{i}\chi k_\beta Q_{\alpha\beta}$, where $\mathbf{k}$ is the wave vector. This scaling demonstrates that nematopolar coupling vanishes in the limit $k \to 0$. Thus, long-wavelength velocity fluctuations cannot feed back to polar ordering and, in turn, be amplified, thereby suppressing the scale-free instability typical in dipolar active suspensions [2].

Nonlinear simulations. We next study the long-time dynamics and pattern formation resulting from the instabilities beyond the linear theory. To this end, we perform three-dimensional (3D) nonlinear numerical simulations whereby we integrate Eqs. (13)–(15) in conjunction with the Stokes equation for the mean-field velocity $\mathbf{u}(\mathbf{x})$ [39]. The governing equations are solved in a triply periodic domain using a pseudospectral method with a fourth-order accurate Runge-Kutta scheme for time stepping [44]. Here, we have retained the first three moments of our particle distribution function and have approximated the higher-order moments $\{\mathbf{R}, \mathbf{S}\}$ using an appropriate closure following [45,46].

We initiate our simulations close to isotropy with long-wavelength perturbations in all the evolved fields. The box size is chosen such that the unstable wave numbers are incorporated in the simulation domain. The simulations reveal emergent and self-sustained large-scale flows, emergent polar order, and pronounced concentration fluctuations in the suspension (Fig. 3). The collective patterned states with density fluctuations are truly nonlinear and are not predicted by the linear theory. Similar to bacterial suspensions, striation and bands in the concentration field appear because it is advected by the polarity field $\chi\mathbf{n}$, which is not divergence free; particles accumulate in regions where $\boldsymbol{\nabla} \cdot (c\mathbf{n}) < 0$.

Conclusion. Through a combination of theory, stability analysis, and large-scale simulations, we have uncovered a previously unknown pathway to pattern formation and collective dynamics in bulk Stokesian suspensions of torque-driven chiral particles. Remarkably, the instability we observe is intrinsically tied to self-propulsion and, therefore, to the microscopic chirality of the constituent particles. This mechanism stands in contrast to well-studied active suspensions,

where self-propulsion plays only a minor role [48] and can even stabilize alignment instabilities [49,50]. Our micro-macro framework further shows that self-propulsion naturally generates nematopolar couplings [42,51], which are essential for driving this novel class of instabilities. While our work is inspired by torque-driven systems such as Quincke rollers, the present study focuses on bulk suspensions that preserve full rotational symmetry on $\mathbb{S}^2$. Exploring how a globally imposed field alters the resulting collective dynamics is a natural direction for future work. More broadly, we expect our findings will inspire new approaches in the design and exploration of torque-driven active suspensions [52] with potential implications for transport using actuated nanobots [11,53]. Our theoretical framework enables us to probe the rheology of these suspensions and will be used to develop a mechanistic understanding of the emergent odd viscosity in parity-breaking bulk chiral fluids [54,55].

Acknowledgments. We thank Anke Lindner and Jasmin Imran Alsous for feedback on this work. B.C. acknowledges the support of the Department of Atomic Energy, Government of India, under Project No. RTI4019. Part of the work was carried out at ESPCI, Paris, supported by the SSHN fellowship (2024). S.C. thanks Vinay Kumar and Santhiya P S for their help with Dedalus and Paraview.

Data availability. The data that support the findings of this article are openly available [56].

[1] R. A. Simha and S. Ramaswamy, Hydrodynamic fluctuations and instabilities in ordered suspensions of self-propelled particles, Phys. Rev. Lett. **89**, 058101y (2002).
[2] D. Saintillan and M. J. Shelley, Instabilities and pattern formation in active particle suspensions: Kinetic theory and continuum simulations, Phys. Rev. Lett. **100**, 178103 (2008).
[3] G. Subramanian and D. L. Koch, Critical bacterial concentration for the onset of collective swimming, J. Fluid Mech. **632**, 359 (2009).
[4] A. Baskaran and M. C. Marchetti, Statistical mechanics and hydrodynamics of bacterial suspensions, Proc. Natl. Acad. Sci. USA **106**, 15567 (2009).
[5] M. C. Marchetti, J.-F. Joanny, S. Ramaswamy, T. B. Liverpool, J. Prost, M. Rao, and R. A. Simha, Hydrodynamics of soft active matter, Rev. Mod. Phys. **85**, 1143 (2013).
[6] R. Alert, J.-F. Joanny, and J. Casademunt, Universal scaling of active nematic turbulence, Nat. Phys. **16**, 682 (2020).
[7] S. Ramaswamy, The mechanics and statistics of active matter, Annu. Rev. Condens. Matter Phys. **1**, 323 (2010).
[8] D. Saintillan and M. J. Shelley, Theory of active suspensions, in *Complex Fluids in Biological Systems: Experiment, Theory, and Computation* (Springer, Berlin, 2014), pp. 319–355.
[9] R. Alert, J. Casademunt, and J.-F. Joanny, Active turbulence, Annu. Rev. Condens. Matter Phys. **13**, 143 (2022).
[10] X. M. de Wit, M. Fruchart, T. Khain, F. Toschi, and V. Vitelli, Pattern formation by turbulent cascades, Nature (London) **627**, 515 (2024).
[11] A. Ghosh and P. Fischer, Controlled propulsion of artificial magnetic nanostructured propellers, Nano Lett. **9**, 2243 (2009).
[12] R. Goyal, J. Behera, P. Mandal, and A. Ghosh, Externally controlled intermittent randomization enables complex navigation of multiple nanobots, Nat. Commun. **16**, 2700 (2025).
[13] D. Banerjee, A. Souslov, A. G. Abanov, and V. Vitelli, Odd viscosity in chiral active fluids, Nat. Commun. **8**, 1573 (2017).
[14] A. Maitra, Activity unmasks chirality in liquid-crystalline matter, Annu. Rev. Condens. Matter Phys. **16**, 275 (2025).
[15] N. Darnton, L. Turner, K. Breuer, and H. C. Berg, Moving fluid with bacterial carpets, Biophys. J. **86**, 1863 (2004).
[16] D. J. Smith, J. R. Blake, and E. A. Gaffney, Fluid mechanics of nodal flow due to embryonic primary cilia, J. R. Soc. Interface **5**, 567 (2008).
[17] S. Fürthauer, M. Strempel, S. W. Grill, and F. Jülicher, Active chiral processes in thin films, Phys. Rev. Lett. **110**, 048103 (2013).
[18] S. R. Naganathan, S. Fürthauer, M. Nishikawa, F. Jülicher, and S. W. Grill, Active torque generation by the actomyosin cell cortex drives left–right symmetry breaking, eLife **3**, e04165 (2014).
[19] L. Meißner, L. Niese, and S. Diez, Helical motion and torque generation by microtubule motors, Curr. Opin. Cell Biol. **88**, 102367 (2024).
[20] E. Lauga, *The Fluid Dynamics of Cell Motility* (Cambridge University Press, Cambridge, UK, 2020), Vol. 62.
[21] V. Soni, E. S. Bililign, S. Magkiriadou, S. Sacanna, D. Bartolo, M. J. Shelley, and W. T. Irvine, The odd free surface flows of a colloidal chiral fluid, Nat. Phys. **15**, 1188 (2019).
[22] A. Maitra, M. Lenz, and R. Voituriez, Chiral active hexatics: Giant number fluctuations, waves, and destruction of order, Phys. Rev. Lett. **125**, 238005 (2020).
[23] S. J. Kole, G. P. Alexander, S. Ramaswamy, and A. Maitra, Layered chiral active matter: Beyond odd elasticity, Phys. Rev. Lett. **126**, 248001 (2021).
[24] A. Maitra and M. Lenz, Spontaneous rotation can stabilise ordered chiral active fluids, Nat. Commun. **10**, 920 (2019).
[25] P. Patra, K. Beyer, A. Jaiswal, A. Battista, K. Rohr, F. Frischknecht, and U. S. Schwarz, Collective migration reveals mechanical flexibility of malaria parasites, Nat. Phys. **18**, 586 (2022).
[26] P. Digregorio, I. Pagonabarraga, and F. V. Reyes, Phase separation in a chiral active fluid of inertial self-spinning disks, arXiv:2504.08533.
[27] Y. Kuroda, T. Kawasaki, and K. Miyazaki, Singular density correlations in chiral active fluids in three dimensions, Phys. Rev. E **112**, 045426 (2025).
[28] D. Banerjee and R. Alert, Active screws: Emergent active chiral nematics of spinning self-propelled rods, arXiv:2410.12263.
[29] P. M. Vlahovska, Electrohydrodynamics of drops and vesicles, Annu. Rev. Fluid Mech. **51**, 305 (2019).
[30] Q. Brosseau, G. Hickey, and P. M. Vlahovska, Electrohydrodynamic Quincke rotation of a prolate ellipsoid, Phys. Rev. Fluids **2**, 014101 (2017).
[31] T. Lefranc, A. Dinelli, C. Fernández-Rico, R. Dullens, J. Tailleur, and D. Bartolo, Quorum sensing and absorbing phase transitions in colloidal active matter, Phys. Rev. X **15**, 031050 (2025).
[32] D. Das and E. Lauga, Active particles powered by Quincke rotation in a bulk fluid, Phys. Rev. Lett. **122**, 194503 (2019).

[33] G. B. Jeffery, The motion of ellipsoidal particles immersed in a viscous fluid, Proc. R. Soc. Lond. Ser. A **102**, 161 (1922).

[34] M. Dalwadi, C. Moreau, E. Gaffney, K. Ishimoto, and B. Walker, Generalised Jeffery's equations for rapidly spinning particles. Part 1. Spheroids, J. Fluid Mech. **979**, A1 (2024).

[35] M. Dalwadi, C. Moreau, E. Gaffney, B. Walker, and K. Ishimoto, Generalised Jeffery's equations for rapidly spinning particles. Part 2. Helicoidal objects with chirality, J. Fluid Mech. **979**, A2 (2024).

[36] Marcos, H. C. Fu, T. R. Powers, and R. Stocker, Separation of microscale chiral objects by shear flow, Phys. Rev. Lett. **102**, 158103 (2009).

[37] G. Batchelor, The stress system in a suspension of force-free particles, J. Fluid Mech. **41**, 545 (1970).

[38] J. Dahler and L. Scriven, Theory of structured continua I. General consideration of angular momentum and polarization, Proc. R. Soc. Lond. Ser. A **275**, 504 (1963).

[39] See Supplemental Material at http://link.aps.org/supplemental/10.1103/9kfb-c51g for details on the modeling, numerical methods, and additional calculations supporting the results in the main text.

[40] I. Lavi, R. Alert, J.-F. Joanny, and J. Casademunt, Nonlinear spontaneous flow instability in active nematics, Phys. Rev. Lett. **134**, 238301 (2025).

[41] I. Lavi, R. Alert, J.-F. Joanny, and J. Casademunt, Dynamical arrest in active nematic turbulence, arXiv:2407.15149.

[42] M. E. Cates and J. Tailleur, When are active Brownian particles and run-and-tumble particles equivalent? Consequences for motility-induced phase separation, Europhys. Lett. **101**, 20010 (2013).

[43] D. Das and D. Saintillan, On the absence of collective motion in a bulk suspension of spontaneously rotating dielectric particles, Soft Matter **19**, 6825 (2023).

[44] K. J. Burns, G. M. Vasil, J. S. Oishi, D. Lecoanet, and B. P. Brown, Dedalus: A flexible framework for numerical simulations with spectral methods, Phys. Rev. Res. **2**, 023068 (2020).

[45] M. Theillard and D. Saintillan, Computational mean-field modeling of confined active fluids, J. Comput. Phys. **397**, 108841 (2019).

[46] S. Weady, D. B. Stein, and M. J. Shelley, Thermodynamically consistent coarse-graining of polar active fluids, Phys. Rev. Fluids **7**, 063301 (2022).

[47] H. H. Wensink, J. Dunkel, S. Heidenreich, K. Drescher, R. E. Goldstein, H. Löwen, and J. M. Yeomans, Meso-scale turbulence in living fluids, Proc. Natl. Acad. Sci. USA **109**, 14308 (2012).

[48] T. Sanchez, D. T. Chen, S. J. DeCamp, M. Heymann, and Z. Dogic, Spontaneous motion in hierarchically assembled active matter, Nature (London) **491**, 431 (2012).

[49] R. Chatterjee, N. Rana, R. A. Simha, P. Perlekar, and S. Ramaswamy, Inertia drives a flocking phase transition in viscous active fluids, Phys. Rev. X **11**, 031063 (2021).

[50] L. Ohm and M. J. Shelley, Weakly nonlinear analysis of pattern formation in active suspensions, J. Fluid Mech. **942**, A53 (2022).

[51] F. Vafa and A. Doostmohammadi, Phase diagram, confining strings, and a new universality class in nematopolar matter, arXiv:2501.04769.

[52] P. Chen, S. Weady, S. Atis, T. Matsuzawa, M. J. Shelley, and W. T. Irvine, Self-propulsion, flocking and chiral active phases from particles spinning at intermediate Reynolds numbers, Nat. Phys. **21**, 146 (2025).

[53] S. Chen, D. E. Fan, P. Fischer, A. Ghosh, K. Göpfrich, R. Golestanian, H. Hess, X. Ma, B. J. Nelson, T. Patiño Padial, *et al.*, A roadmap for next-generation nanomotors, Nat. Nanotechnol. **20**, 990 (2025).

[54] M. Fruchart, C. Scheibner, and V. Vitelli, Odd viscosity and odd elasticity, Annu. Rev. Condens. Matter Phys. **14**, 471 (2023).

[55] C.-T. Lee, T. Lubensky, and T. Markovich, Odd elasticity in disordered chiral active materials, arXiv:2508.04468.

[56] https://github.com/bratochakra/Chiral_Suspension_2026.